Applied Energy 134 (2014) 65–74

Contents lists available at ScienceDirect

Applied Energy

journal homepage: www.elsevier.com/locate/apenergy

Development and validation of a new TRNSYS type for the simulation of thermoelectric generators

E. Massaguer *, A. Massaguer, L. Montoro, J.R. Gonzalez

Department of Mechanical Engineering and Industrial Construction, University of Girona, C. de Maria Aurèlia Capmany, 61, 17071 Girona, Spain

HIGHLIGHTS

- A new TRNSYS component for simulation of thermoelectric generators is developed.
- A TEG model is proposed and validated under transient and steady-state conditions.
- The results have approved the reasonability of the new component.

ARTICLE INFO

Article history:
Received 29 March 2014
Received in revised form 28 May 2014
Accepted 1 August 2014
Available online 23 August 2014

Keywords:
Thermoelectric generator
TEG
TRNSYS
Computational model
Power generation

ABSTRACT

Thermoelectric generators (TEGs) make use of the Seebeck effect in semiconductors for the direct conversion of heat into electrical energy, being of particular interest for high reliability systems or for waste heat recovery. Although several TEG models can be found in the literature, many of them not offer a theoretical solution because they are based on steady-state solutions or they are assuming fixed parameters as boundary conditions. Consequently, to assess and optimize thermoelectric generators in real applications a numerical transient simulation tool, which takes into account the whole energy system, is mandatory. For that purpose, a new TRNSYS type is developed. This TEG component, which can be used as a design tool, is presented in this paper and validated using experimental data.

The results show that the proposed component is able to cope with both thermal and electrical dynamics. The comparison between theoretic and experimental results has approved the reasonability of the new component. The normalized root mean square errors are 3.53% and 2.33% for temperature difference between hot and cold sides and electrical output power, respectively.

1. Introduction

A thermoelectric power generator is a solid-state device that provides direct energy conversion from thermal energy, due to a temperature gradient, into electrical energy based on Seebeck effect. Also, they can work in reverse and use electrical energy to create a temperature gradient for cooling or heating applications. The absence of moving parts, wide range of operating temperatures, scalability, and modular capabilities makes thermoelectricity attractive for a wide variety of applications, such as power for remote control and monitoring of oil or gas pipelines and production facilities, automotive waste heat recovery, power for navigational aids, spacecraft radioisotope power supply, telecommunications systems and cathodic protection, and other energy recovery processes [1–6]. Thermoelectric devices have relatively low efficiencies but there have been recent advances in thermoelectric materials potentially opening the door to new power applications [7,8]. As material advancements continue and a wider range of power generation applications will be considered, module and system level modelling becomes critical for the design of the next generation of thermoelectric systems.

Although several models for TEG modules can be found in the literature [9–16], many of them not offer a theoretical solution because their governing equations are based on steady-state solutions or they are assuming fixed temperatures as boundary conditions at both sides of the TEG. Moreover, almost none of them have studied the transient effects of load resistance. Complete transient analyses are seldom presented and just a few have already provided a complete mathematical solution of the heat conduction equation for TEG devices [13–15].

This study attempts to fill the existing gap in the simulation of thermoelectric generation through the development of a new component that can be used in TRNSYS software. TRNSYS [17],

* Corresponding author. Tel.: +34 972 418 489; fax: +34 972 418 098.
E-mail address: Eduard.massaguer@udg.edu (E. Massaguer).

http://dx.doi.org/10.1016/j.apenergy.2014.08.010
0306-2619/

Nomenclature

Abbreviation

TEG	thermoelectric generator

Symbols

n	number of thermocouples
α	Seebeck coefficient (V/K)
σ	electrical resistivity (Ω m)
e	length (m)
A	cross sectional area (m^2)
ρ	material density ($kg(m^3)$)
S	specific heat capacity (J/kg K)
λ	thermal conductivity (W/m K)
K	thermal conductance (W/K)
C	thermal capacity (J/K))
h	convective heat transfer coefficient (W/m^2 K)
Q	heat rate (W)
V	electric voltage (V)
I	electric current (A)
P	electric power (W)
η	efficiency (%)
R	electric resistance (Ω)
T	temperature (K)
y	axis coordinate (m)
t	time (s)

Subscript

hp	hot plate
$tc_{1,2}$	thermal compound
ce	ceramic substrate
cp	cold plate
cb	water-cooling block
h	hot side
c	cold side
p	p-type semiconductor
n	n-type semiconductor
in	input
L	load resistance
c_∞	cooling water
oc	open circuit
max	maximum
ss	steady-state

developed at the University of Wisconsin, is a transient systems simulation program with a modular structure. It recognizes a system description language in which the user specifies the components that constitute the system and the manner in which they are connected. The TRNSYS library includes many of the components commonly found in thermal and electrical energy systems, as well as component routines to handle input of weather data or other time-dependent forcing functions and output of simulation results. The modular nature of TRNSYS gives the program flexibility, and facilitates the addition to the program of mathematical models not included in the standard TRNSYS library. TRNSYS is well suited to detailed analyses of any system whose behaviour is dependent on the passage of time. It has become reference software for researchers and engineers around the world. Main applications include: solar systems (solar thermal and photovoltaic systems), low energy buildings, HVAC systems, renewable energy systems, cogeneration, fuel cells and more.

Full integration of the new component within the TRNSYS simulation package is another advantage of this study, which makes it more applicable for designers in both the design and commissioning of waste energy harvesting systems. The incorporation of the TEG model into standard TRNSYS library will allow users to simulate TEGs coupled to many different thermal facilities and applications (e.g. solar thermal systems, geothermal systems and more). Because of the mentioned benefits, TRNSYS is chosen to implement the new component.

The objective of this work is to develop a computational model capable to simulate the electro-thermal dynamics of a TEG system into TRNSYS software. The new component is fully analysed and validated under steady and transient states with data obtained from the experimental setup.

2. TEG modelling

A TEG device in essence is a thermopile composed of a number of p- and n-type semiconductor pairs connected electrically in series. Heat carries the majority carriers from one junction to the other producing a current and voltage. By placing many PN couples in series electrically and in parallel thermally, a TEG module generates an open-circuit voltage proportional to the temperature differential across the elements.

According to Seebeck, Peltier and Thomson effects, the TEG power generation depends mainly on both temperature differential across the semiconductor elements and electrical load connected (i.e. changes of the temperature difference lead to changes of the open-circuit voltage, and the TEG output performance will change as well). Therefore, the unsteady-state heat transfer model is built to solve the TEG temperature distribution. Thereafter, the TEG power and performance outputs can be determined.

Similar with Gou [12,21], Kim [20], Nguyen [14] and Rodríguez [19], the basic configuration of the thermoelectric study follows the general design illustrated in Fig. 1.

A thermoelectric module is sandwiched between electrical heater and water-cooled heat exchanger that can be treated as a convective heat transfer system. The TEG consists of certain number of semiconductors, corresponding solder layers, conducting strips and thermal insulation material. In order to electrically isolate the module, a ceramic substrate is located both sides of the TEG. A thermal compound increases the thermal conductivity of the interfaces by filling microscopic air-gaps between ceramic substrates and aluminium plates and TEG and ceramic substrates, respectively. At the same time, hot and cold plates allow to introduce temperature sensors on the experimental set up.

2.1. Assumptions and boundary conditions

In the analytical assessing, the thermal conductivity, electric conductivity, and Seebeck coefficient of semiconductors are all assumed to be temperature-independent, and adiabatic boundary conditions were supposed on the side surfaces of TEG element. Thermal conductivities, electrical resistivity, and specific heat capacities of non-thermoelectric materials are supposed constants within the operating temperature range.

Due to the fact that this study is focused on low-temperature system, the Thomson effect could be neglected [17]. Besides, initial temperature of the system is equal to ambience temperature, this means that temperatures at both sides of the TEG element are the

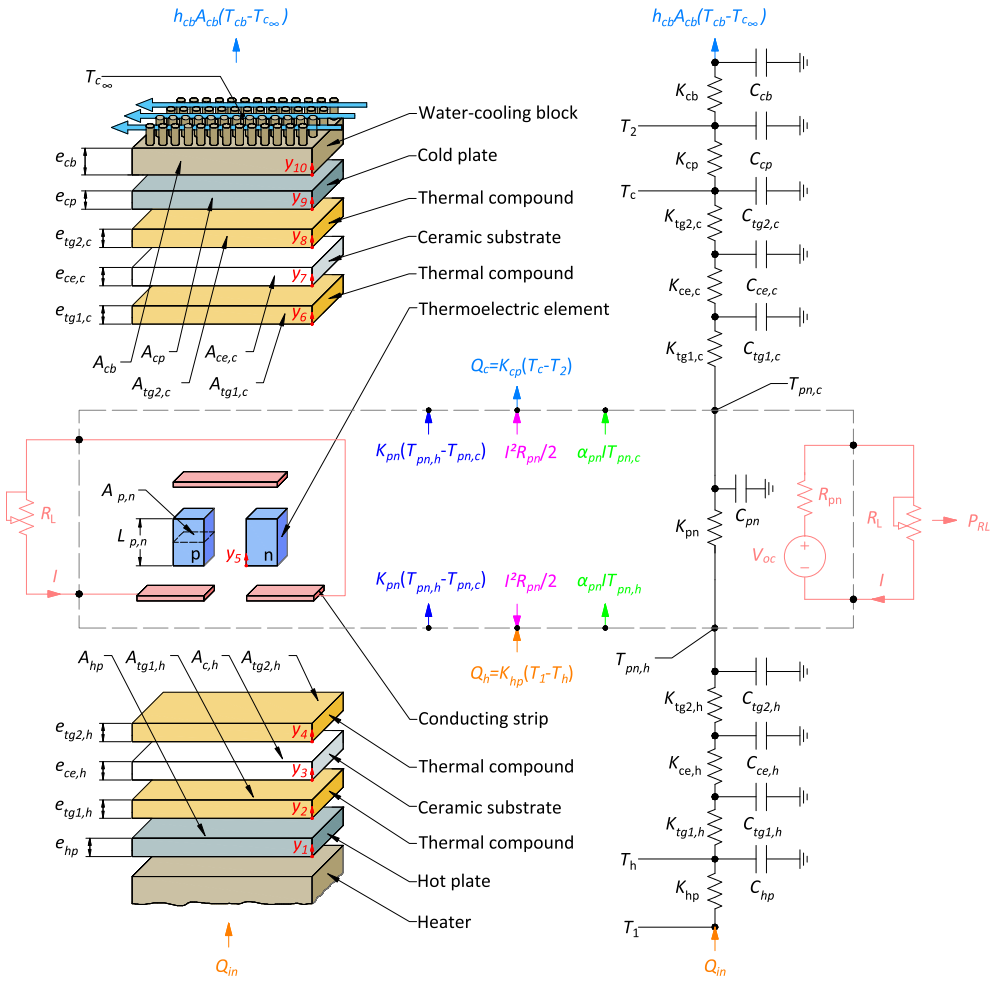

Fig. 1. One-dimensional heat transfer model of thermoelectric generator.

same, and consequently initial output data is zero. Finally, an instantaneous response to electrical load transients is considered [13].

The heat leakage through the solder layer and conducting strips are neglected. The flow of heat and current in the system are assumed one-dimensional. All materials are assumed homogeneous and isotropic. Finally, heat losses due to radiation and transverse convection are neglected.

2.2. Governing equations

In thermoelectric devices, both refrigeration and generation applications, the internal and external nodal temperatures of TEG cannot be determined analytically without knowing the heat flux due to the thermoelectric effects. The reasons are the nonlinearities of the thermoelectricity and heat transfer equations.

The model solves the nonlinearities using finite difference and Newton–Raphson methods, which calculates the temperature at different nodes separated in space by a discrete distance. In the transient state, the temperatures of these points are calculated at discrete periods of time and the temperatures for all the nodes are recalculated at the end of this time interval. Using the implicit finite difference method, the values of heat flux can be determined using the values of the temperatures of the time step before.

According to heat conduction theory, the one-dimensional unsteady heat conduction equation of non-thermoelectric elements can be shown as:

$$\rho_i S_i \frac{\partial T_i}{\partial t} = \lambda_i \frac{\partial^2 T_i}{\partial y_i^2} \tag{1}$$

where ρ, S and λ are density, specific heat capacity and thermal conductivity, respectively, t and y are time and axis coordinate, respectively. The subscript i determines the heat transfer related to node i. As found in the referenced literature [13,19], the thermal–electrical analogy is useful in the analysis of complicated unsteady heat transfer problems, which can be understood by creating an electric circuit like Fig. 1 with following equations:

$$K_i = \frac{\lambda_i A_i}{e_i} \tag{2}$$

$$C_i = \rho_i S_i A_i e_i \tag{3}$$

where K_i and C_i are the thermal conductance and thermal capacity associated with each node i.

The governing equations for p- and n-type thermoelectric elements involve three basic effects, Seebeck effect, Peltier effect and Thomson effect. Besides, there are two accessorial effects, Joule effect and Fourier effect. Gou [12] explained that Peltier heat generates on the two sides of semiconductor and Joule heat can be regarded as flowing equally to the two sides of conductors, so they can be disposed as a boundary heat fluxes. Thomson heat is small enough to be neglected since it is a second-round effect. So the TEG inner unsteady-state heat transfer equation can be translated also as Eq. (1).

The boundary condition applied at the hot plate surface, $y_1 = 0$, corresponds to the applied heat from electrical heater Q_{in}. On the top surface, $y_{10} = e_{cb}$, the convection boundary equation is employed. The boundary conditions applied to solve the unsteady-state heat transfer Eq. (1) for the system shown in Fig. 1 are listed below.

Between heater and hot plate surface

$$Q_{in} = -\lambda_{hp} A_{hp} \left.\frac{\partial T}{\partial y}\right|_{y_1=0} \tag{4}$$

Between hot plate and thermal compound

$$-\lambda_{hp} A_{hp} \left.\frac{\partial T}{\partial y}\right|_{y_1=e_{hp}} = -\lambda_{tc1,h} A_{tc1,h} \left.\frac{\partial T}{\partial y}\right|_{y_2=0} \tag{5}$$

Between thermal compound and ceramic plate

$$-\lambda_{tc1,h} A_{tc1,h} \left.\frac{\partial T}{\partial y}\right|_{y_2=e_{tc1,h}} = -\lambda_{ce,h} A_{ce,h} \left.\frac{\partial T}{\partial y}\right|_{y_3=0} \tag{6}$$

Between ceramic plate and thermal compound

$$-\lambda_{ce,h} A_{ce,h} \left.\frac{\partial T}{\partial y}\right|_{y_3=e_{ce,h}} = -\lambda_{tc2,h} A_{tc2,h} \left.\frac{\partial T}{\partial y}\right|_{y_4=0} \tag{7}$$

Between thermal compound and thermoelectric element

$$-\lambda_{tc2,h} A_{tc2,h} \left.\frac{\partial T}{\partial y}\right|_{y_4=e_{tc2,h}} = -\lambda_{pn} A_{pn} \left.\frac{\partial T}{\partial y}\right|_{y_5=0} + \alpha_{pn} I T_{pn,h} - \frac{1}{2} I^2 R_{pn} \tag{8}$$

Between thermoelectric element and thermal compound

$$-\lambda_{pn} A_{pn} \left.\frac{\partial T}{\partial y}\right|_{y_5=e_{pn}} + \alpha_{pn} I T_{pn,c} + \frac{1}{2} I^2 R_{pn} = -\lambda_{tc1,c} A_{tc1,c} \left.\frac{\partial T}{\partial y}\right|_{y_6=0} \tag{9}$$

Between thermal compound and ceramic plate

$$-\lambda_{tc1,c} A_{tc1,c} \left.\frac{\partial T}{\partial y}\right|_{y_6=e_{tc1,c}} = -\lambda_{ce,c} A_{ce,c} \left.\frac{\partial T}{\partial y}\right|_{y_7=0} \tag{10}$$

Between ceramic plate and thermal compound

$$-\lambda_{ce,c} A_{ce,c} \left.\frac{\partial T}{\partial y}\right|_{y_7=e_{ce,c}} = -\lambda_{tc2,c} A_{tc2,c} \left.\frac{\partial T}{\partial y}\right|_{y_8=0} \tag{11}$$

Between thermal compound and cold plate

$$-\lambda_{tc2,c} A_{tc2,c} \left.\frac{\partial T}{\partial y}\right|_{y_8=e_{tc2,c}} = -\lambda_{cp} A_{cp} \left.\frac{\partial T}{\partial y}\right|_{y_9=0} \tag{12}$$

Between cold plate and water-cooling block

$$-\lambda_{cp} A_{cp} \left.\frac{\partial T}{\partial y}\right|_{y_9=e_{cp}} = -\lambda_{cb} A_{cb} \left.\frac{\partial T}{\partial y}\right|_{y_{10}=0} \tag{13}$$

Between water-cooling block and cooling fluid

$$-\lambda_{cb} A_{cb} \left.\frac{\partial T}{\partial y}\right|_{y_{10}=e_{cb}} = h_{cb} A_{cb} (T_{cb} - T_{c\infty}) \tag{14}$$

With

$$\alpha_{pn} = n(\alpha_p - \alpha_n) \tag{15}$$

$$\lambda_{pn} = n(\lambda_p + \lambda_n) \tag{16}$$

$$A_{pn} = n(A_p + A_n) \tag{17}$$

$$R_{pn} = n\left(\frac{\sigma_p e_p}{A_p} + \frac{\sigma_n e_n}{A_n}\right) \tag{18}$$

$$I = \frac{\alpha_{pn}(T_{pn,h} - T_{pn,c})}{R_{pn} + R_L} \tag{19}$$

where λ_{hp}, λ_{cp}, λ_{tc1}, λ_{ce}, λ_{tc2}, λ_{cb} and λ_{pn} are thermal conductivities of hot plate, cold plate, external thermal compound, ceramic plate, internal thermal compound, water-cooling block and thermoelectric generator, respectively; e_{hp}, e_{cp}, e_{tc1}, e_{ce}, e_{tc2}, e_{cb} and e_{pn} are lengths of hot plate, cold plate, external thermal compound, ceramic plate, internal thermal compound, water-cooling block and thermoelectric generator, respectively; A_{hp}, A_{cp}, A_{tc1}, A_{ce}, A_{tc2}, A_{cb} and A_{pn} are cross sectional areas of hot plate, cold plate, external thermal compound, ceramic plate, internal thermal compound, water-cooling block and thermoelectric generator, respectively; $T_{pn,h}$ and $T_{pn,c}$ are temperatures of hot and cold side of semiconductor, respectively; T_{cb} and $T_{c\infty}$ are cold side temperature of water-cooling block and cooling fluid temperature, respectively; h_{cb} is coefficient of convective heat transfer; I is electrical current flowing through the thermoelectric circuit; R_{pn} and α_{pn} are the electric resistance and Seebeck coefficient of TEG, respectively; n is the number of semiconductor thermocouples; α_n, α_p, λ_n, λ_p, A_n, A_p, e_n, e_p, σ_n, σ_p, are the Seebeck coefficients, thermal conductivities, cross sectional areas, lengths and electrical resistivities of p- and n-type elements.

Once heat transfer equation system, Eqs. (4)–(14) and additionally Eqs. (15)–(19), is solved using implicit finite difference method, the nodal temperatures on hot and cold side of the semiconductor are found for every time step. Consequently, the electrical and thermal outputs can be obtained every time step. According to Seebeck effect the open circuit electromotive force generated is expressed as follows

$$V_{oc}(t) = \alpha_{pn}(T_{pn,h}(t) - T_{pn,c}(t)) \tag{20}$$

The output current I and output voltage V_{RL} generated depends on the load resistance R_L and it can be calculated following Eqs. (16) and (18), respectively.

$$V_{R_L}(t) = \frac{\alpha_{pn}(T_{pn,h}(t) - T_{pn,c}(t))R_L}{R_{pn} + R_L} \tag{21}$$

Besides, short circuit current also can be obtained

$$I_{sc}(t) = \frac{\alpha_{pn}(T_{pn,h}(t) - T_{pn,c}(t))}{R_{pn}} \tag{22}$$

So the output power when R_L is connected is given by

$$P_{R_L}(t) = V_{R_L} I = \frac{\alpha_{pn}^2 (T_{pn,h}(t) - T_{pn,c}(t))^2 R_L}{(R_{pn} + R_L)^2} \tag{23}$$

Deriving the Eq. (23) with respect to load resistance, $P_{RL}/R_L = 0$, it can be observed that maximum output power will be reached when load electric resistance is equal to the internal electric resistance. Therefore, substituting $R_L = R_{pn}$ into Eq. (23) the maximal output power is

$$P_{max}(t) = \frac{\alpha_{pn}^2 (T_{pn,h}(t) - T_{pn,c}(t))^2}{4R_{pn}} \tag{24}$$

The heat absorption on hot side and heat release on cold side of semiconductor are given by Q_h and Q_c, respectively.

$$Q_h(t) = K_{pn}(T_{pn,h}(t) - T_{pn,c}(t)) + \alpha_{pn} I(t) T_{pn,h}(t) - \frac{1}{2} I^2(t) R_{pn} \tag{25}$$

$$Q_c(t) = K_{pn}(T_{pn,h}(t) - T_{pn,c}(t)) + \alpha_{pn} I(t) T_{pn,c}(t) + \frac{1}{2} I^2(t) R_{pn} \tag{26}$$

Finally, the instantaneous and maximal system efficiency, η and η_{max}, are calculated by Eqs. (27) and (28), respectively.

$$\eta(t) = \frac{P_{R_L}(t)}{Q_h(t)} = \frac{\alpha_{pn}^2 (T_{pn,h}(t) - T_{pn,c}(t))^2 R_L}{(R_{pn} + R_L)^2 K_{pn}(T_{pn,h}(t) - T_{pn,c}(t)) + (R_{pn} + R_L)^2 \alpha_{pn} I(t) T_{pn,h}(t) - \frac{1}{2}(R_{pn} + R_L)^2 I^2(t) R_{pn}} \tag{27}$$

$$\eta_{max}(t)=\frac{P_{max}(t)}{Q_h(t)}=\frac{\alpha_{pn}^2(T_{pn,h}(t)-T_{pn,c}(t))^2}{4R_{pn}K_{pn}(T_{pn,h}(t)-T_{pn,c}(t))+4R_{pn}\alpha_{pn}I(t)T_{pn,h}(t)-2R_{pn}I^2(t)R_{pn}} \quad (28)$$

2.3. Implementation in TRNSYS environment

The TRNSYS software package has been used extensively for thermal system analysis. It has a modular structure and consists of individual subroutines that represent real physical devices or utility components. The components can be connected together to form complex systems.

TRNSYS uses a modular approach to solve thermal energy systems. Basically, it is an equation-solving program based on standard numerical techniques, which provides different subroutines to find analytical solution to the set of equations. However, only a first-order linear differential equation solver is provided. Therefore, a subroutine for solving nonlinear differential equations of Section 2.2 using the finite difference and the Newton–Raphson methods is programmed in Fortran.

Fig. 2 shows the TRNSYS project created to simulate the TEG model. To do so the following input connections has to be established:

- The applied heating rate Q_{in}, obtained from heater specifications.
- The cooling fluid temperature, extracted from experimental data measurements.
- The load resistance R_L, which is used to calculate the output data when specific resistance is connected between positive and negative connections. It may be assigned or leave as default if no load is considered.
- Simulation time step size, which is selected based on the required accuracy of the output data. It also affects to the required computational time.

Additionally, the geometric data and the material properties of the elements of the thermoelectric system studied have to be included into the TEG model as TRNSYS parameter data. All these parameters can be shown in Tables 1 and 2.

After the simulation, the output values obtained from Eqs. (20)–(28) are shown through built-in online plotter.

3. Experimental setup

To compare simulated results with experimental data, the simulation must have the same operating conditions as the experiment. The validation of the TRNSYS Type developed in this study uses experimental data from an especially designed equipment to perform this test. The experimental setup allows establishing parameters required for the simulation of the performance of the TEG, such thermal and electrical transients of different magnitudes.

Fig. 3 shows the schematic of the experiment with a TEG on top of a heat source. The source temperatures, T_1 and T_h, are measured by two K-type thermocouples with diameter of 2 mm placed, as shown in Fig. 1, underneath the TEG and ceramic substrate, respectively. The thermocouple is sealed by conductive thermal compound to assure uniform heat distribution on the TEG hot surface. A water-cooled block cools the top surface of the TEG through a pumped liquid cooling loop consisting of a pump, a heat exchanger and liquid lines. The pump circulates the fluid in the loop, which picks up the heat in the cold plate and dissipates it through the heat exchanger. Two ceramic plates made of alumina (Al_2O_3) are sandwiching the thermo-elements. The temperatures of the top surface (cold side) of the TEG, T_2 and T_c, are also measured by two K-type thermocouples of 2 mm mounted above ceramic substrate and cold plate. The hot and cold plates are treated as heat spreaders to provide a uniform thermal field to both hot and cold sides of TEG module.

Initially, the system is at room temperature, measured as 16.17 °C, and the electrical heater is switched on at its first heating level of Q_{in} = 23.6 W (Case 1). During temperature increase, an external switch intermittently connects and disconnects an electrical load of 2.5 Ω (every 10 s). This allows us to obtain loaded and open-circuit outputs simultaneously. The transient temperatures at the hot and cold surfaces of the TEG, the output voltage and the output current are recorded simultaneously into a digital computer using a data acquisition system (National Instruments-cRIO). The data acquisition is set at a rate of 1 s for about 3500 s at which time the system attains the steady state. Once system reaches the

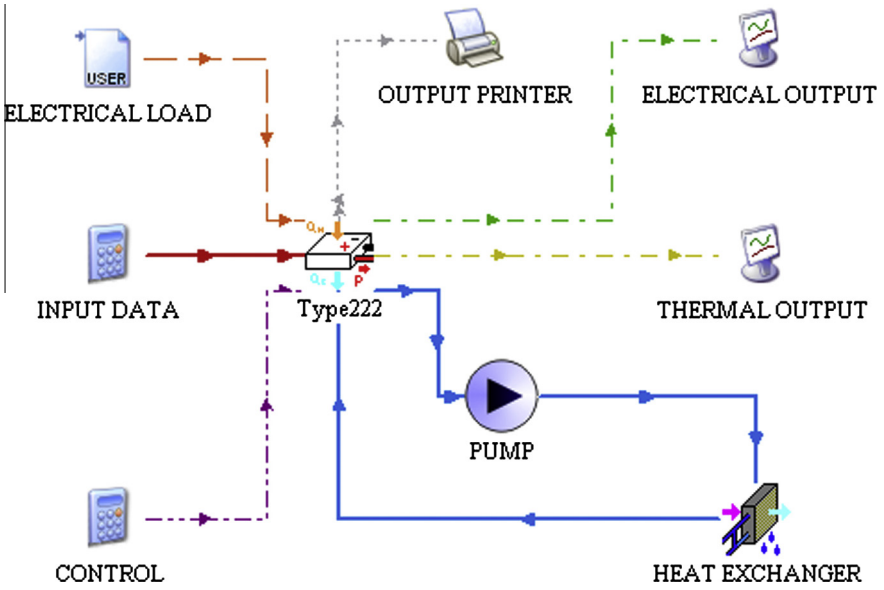

Fig. 2. TRNSYS project created for TEG system behaviour simulation.

Table 1
Thermoelectric parameters for three different cases.

Parameters	Case 1	Case 2	Case 3	Unit	Source
Q_{in}	23.60	33.50	53	W	Measured
$T_{c\infty}$	16.45	17.34	18.20	°C	Measured
R_L	2.5	2.5	2.5	Ω	Measured
α_n	163.546	167.273	171.659	μV/K	Manufacturer
α_p	−178.098	−188.726	−201.897	μV/K	Manufacturer
λ_n	1.510	1.453	1.415	W/m K	Manufacturer
λ_p	1.954	1.925	1.792	W/m K	Manufacturer
σ_n	10.896	12.001	13.767	μΩ m	Manufacturer
σ_p	11.196	13.100	15.910	μΩ m	Manufacturer

Table 2
Properties of materials used in TEG tests.

Parameters	Value	Unit	Source
n	98	–	Measured
e_n	2.54×10^{-3}	m	Measured
e_p	2.54×10^{-3}	m	Measured
e_{hp}	0.02	m	Measured
e_{tc1}	1×10^{-4}	m	Measured
e_{ce}	2.54×10^{-4}	m	Measured
e_{tc2}	1×10^{-4}	m	Measured
e_{cp}	0.02	m	Measured
e_{cb}	0.002	m	Measured
A_n	2.3×10^{-6}	m^2	Measured
A_p	2.3×10^{-6}	m^2	Measured
A_{hp}	7.22×10^{-3}	m^2	Measured
A_{tc1}	8.41×10^{-4}	m^2	Measured
A_{ce}	8.41×10^{-4}	m^2	Measured
A_{tc2}	8.41×10^{-4}	m^2	Measured
A_{cp}	8.41×10^{-4}	m^2	Measured
A_{cb}	12.25×10^{-4}	m^2	Measured
λ_{hp}	180	W/m K	Estimated
λ_{tc1}	2.5	W/m K	Manufacturer
λ_{ce}	36	W/m K	[13]
λ_{tc2}	2.5	W/m K	Manufacturer
λ_{cp}	180	W/m K	Estimated
λ_{cb}	380	W/m K	Estimated
ρ_n	7700	kg/m^3	[18]
ρ_p	7700	kg/m^3	[18]
ρ_{hp}	2700	kg/m^3	Estimated
ρ_{tc1}	2040	kg/m^3	Manufacturer
ρ_{ce}	3975	kg/m^3	[13]
ρ_{tc2}	2040	kg/m^3	Manufacturer
ρ_{cp}	2700	kg/m^3	Estimated
ρ_{cb}	8930	kg/m^3	Estimated
S_n	200	J/kg K	[18]
S_p	200	J/kg K	[18]
S_{hp}	883	J/kg K	Estimated
S_{tc1}	200	J/kg K	Manufacturer
S_{ce}	765	J/kg K	[13]
S_{Ctc2}	200	J/kg K	Manufacturer
S_{cp}	883	J/kgK	Estimated
S_{cb}	385	J/kg K	Estimated
h_{cb}	23781	W/m^2 K	Manufacturer

steady state, the output voltage and current are recorded simultaneously while load resistance varied from 0 Ω to 100 Ω. Table 1 shows the initial values of the test conducted. The experiment is repeated for two additional hot side heat fluxes Q_{in} of 33.5 W (Case 2) and 53 W (Case 3) in order to assess the model at three different temperature gradients.

To assess the TEG behaviour, several thermoelectric properties should be tabulated as a reference. The parameters are determined either according to direct measurement, from manufacturer's data or from the existing literature [12,18]. The geometric parameters and properties of hot and cold plates and water-cooling block are estimated considering that materials used are aluminium and cooper, respectively. Tables 1 and 2 show the properties of materials used in the experimental setup.

In Table 1, the Seebeck coefficient, thermal conductivity and electrical resistivity of the p- and n-type elements are listed at steady-state average temperatures of $\overline{T} = (T_h + T_c)/2$, which are extracted from experimental data. All these three parameters are obtained from manufacturer's datasheet.

Experiments are conducted under following conditions: the temperature of cooling fluid stays between 16.45 °C and 18.20 °C, the air temperature is 16.17 °C and the flow rate of the cooling fluid is 72 l/h.

4. Results and discussion

Based on transient and steady state experiments and TRNSYS simulations, the results and a discussion about their comparison is presented in this section.

4.1. Effects of step changes of supplied heat flow rates

The dynamic response characteristics of temperature difference between hot and cold sides $\Delta T = T_h - T_c$, hot side inlet heat flux Q_h, electric output power P_{RL} and closed-circuit voltage V_{RL} with step changes of supplied heat flow rate Q_{in} are described in Fig. 4. Both the transitory experimental and simulation results are plotted versus the transient time in the same plot. The conditions imposed in the experiment are listed in Table 1.

During the transient, the temperature difference across the TEG device increased until the steady state is achieved. It can be observed that the electric output characteristic is mostly dependent on the temperature difference. The hot side temperature T_h achieved is 99 °C, 140 °C and 216 °C for cases 1, 2 and 3, respectively. Accordingly to experimental data obtained and Eqs. (20)–(28), the higher the temperature difference across the TEG is, the more electrical power generated and the greater output system performance becomes.

4.2. Effects of step changes of load current at constant supplied heat flux

In Fig. 5, the step changes effects of load current under conditions of Table 1 can be observed. The system has been brought to steady-state temperatures of Fig. 4(a). It is very interesting to note the effect that the load current has on the temperature gradient across the device, which is the same obtained in Ref. [15]. The load currents imposed for cases 1–3 are 0.49 A, 0.71 A and 1.01 A, respectively.

Every increase in I leads to a decrease in temperature difference ΔT due to the greater value of the Peltier term of Eqs. (8) and (9). This current increase also produces an increment of hot and cold side heat fluxes. However, as explained in Section 2.2, the maximum output power and efficiency happens only when load resistance is matched with internal resistance.

As it can be appreciated from Fig. 5, the simulation results show good agreement with the experimental results, accurately tracking the electro-thermal coupled effects occurring in the TEG system. The plotted curves of T_h and T_c show that steady-state are not achieved with step changes of 10 s. It also can be shown that parameter variations with load current increase with higher values of supplied heat flux. The low accuracy observed in Fig. 5(c) and (d) may be caused by convection heat losses on hot and cold plates.

4.3. Effects of load resistance variation at steady-state

The variation of performance at steady-state with load resistance is shown in Fig. 6. Three different conditions corresponding

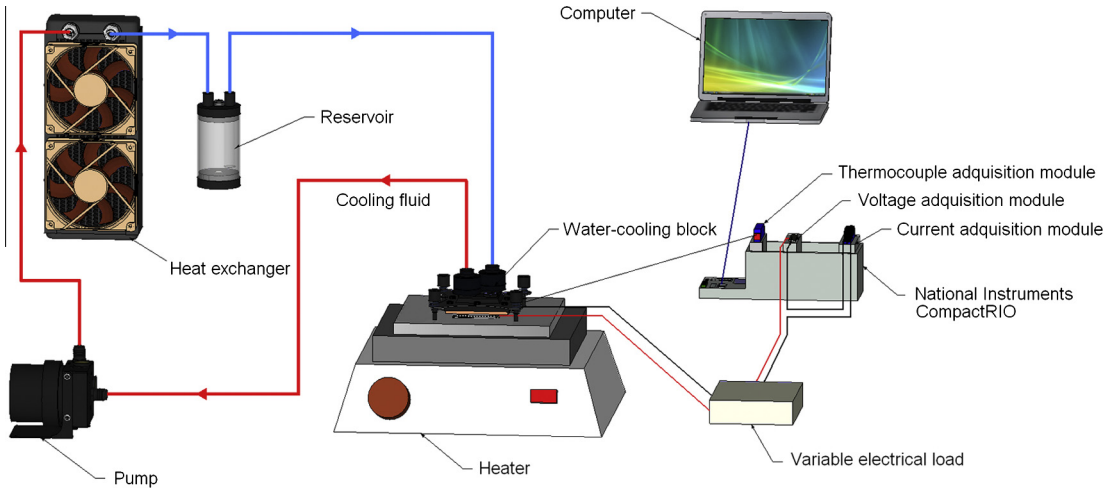

Fig. 3. Experimental test scheme.

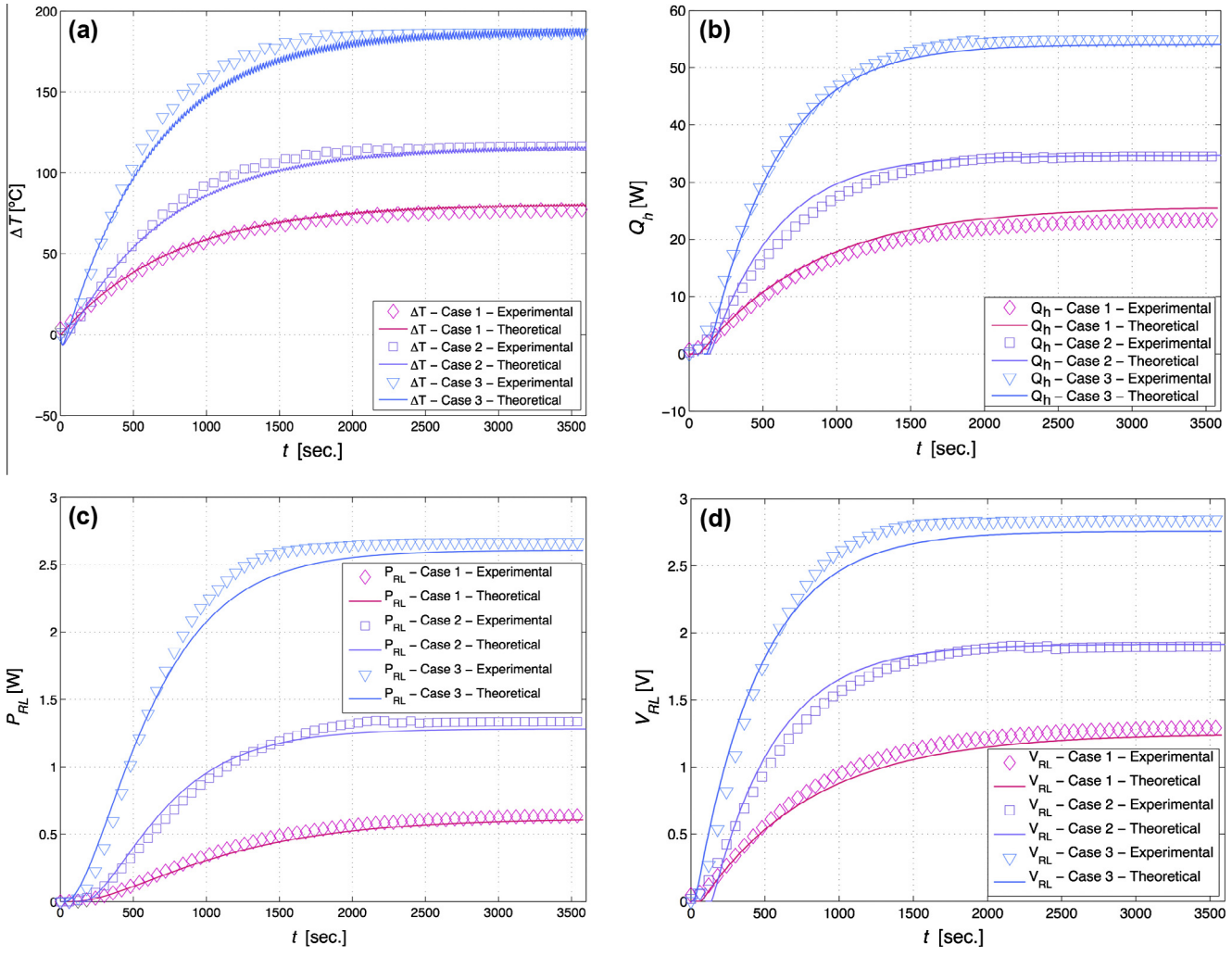

Fig. 4. Correlation of experimental and simulated behaviours of the TEG system under step changes of heat flow rates. (a) Temperature difference between hot and cold sides $\Delta T = T_h - T_c$. (b) Hot side inlet heat flux. (c) Electric output power. (d) Closed-circuit voltage.

to described cases in Table 1 are selected. The system has been brought to the same steady-state temperatures of Fig. 4(a).

Fig. 6 demonstrates that the electrical output is strongly coupled to both the thermal behaviour and the load resistor value. The electric load resistance that produces the maximum electrical power varies with the supplied heat flux. The power generation and system efficiency are the highest when the load resistance value is close to the internal resistance $R_L = R_{pn}$, which is measured

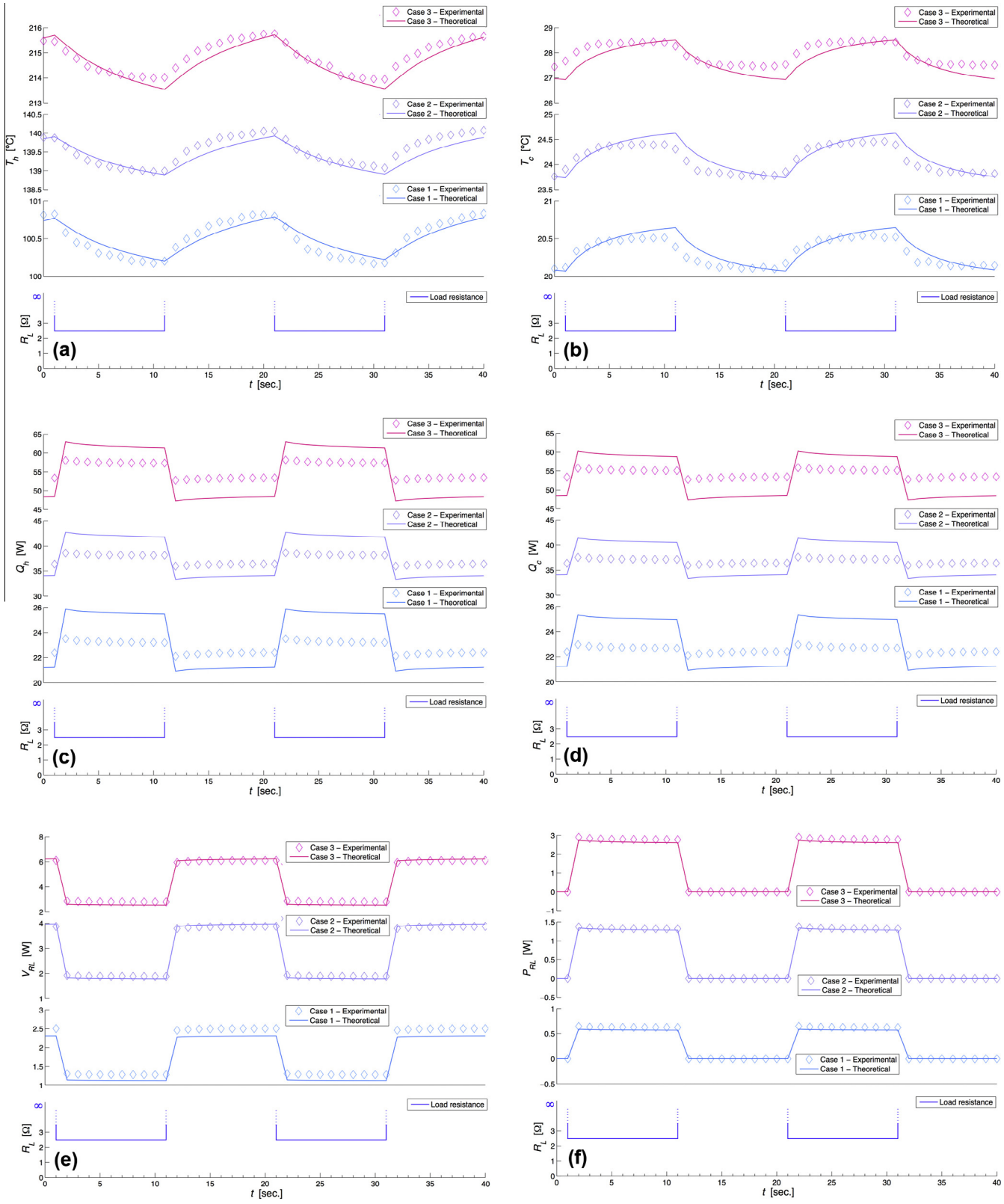

Fig. 5. Correlation of experimental and simulated behaviours of the TEG system under step changes of load current. (a) Hot side temperature. (b) Cold side temperature. (c) Hot side heat flux. (d) Cold side heat flux. (e) Closed-circuit voltage. (f) Electric output power.

to be about 2.5 Ω. As can be shown in Fig. 6(d), the generated power increases to a maximum but then decreases to reach a steady state. The electrical resistances at maximum power points are 2.4 Ω (0.65 W), 2.45 Ω (1.28 W) and 2.9 Ω (2.6 W) for cases 1–3, respectively. Those effects can be observed in the theoretical model as well.

Besides, in Fig. 6(f)–(h) it can be observed that both the hot and cold sides heat fluxes, Q_h and Q_c, decrease with resistance until

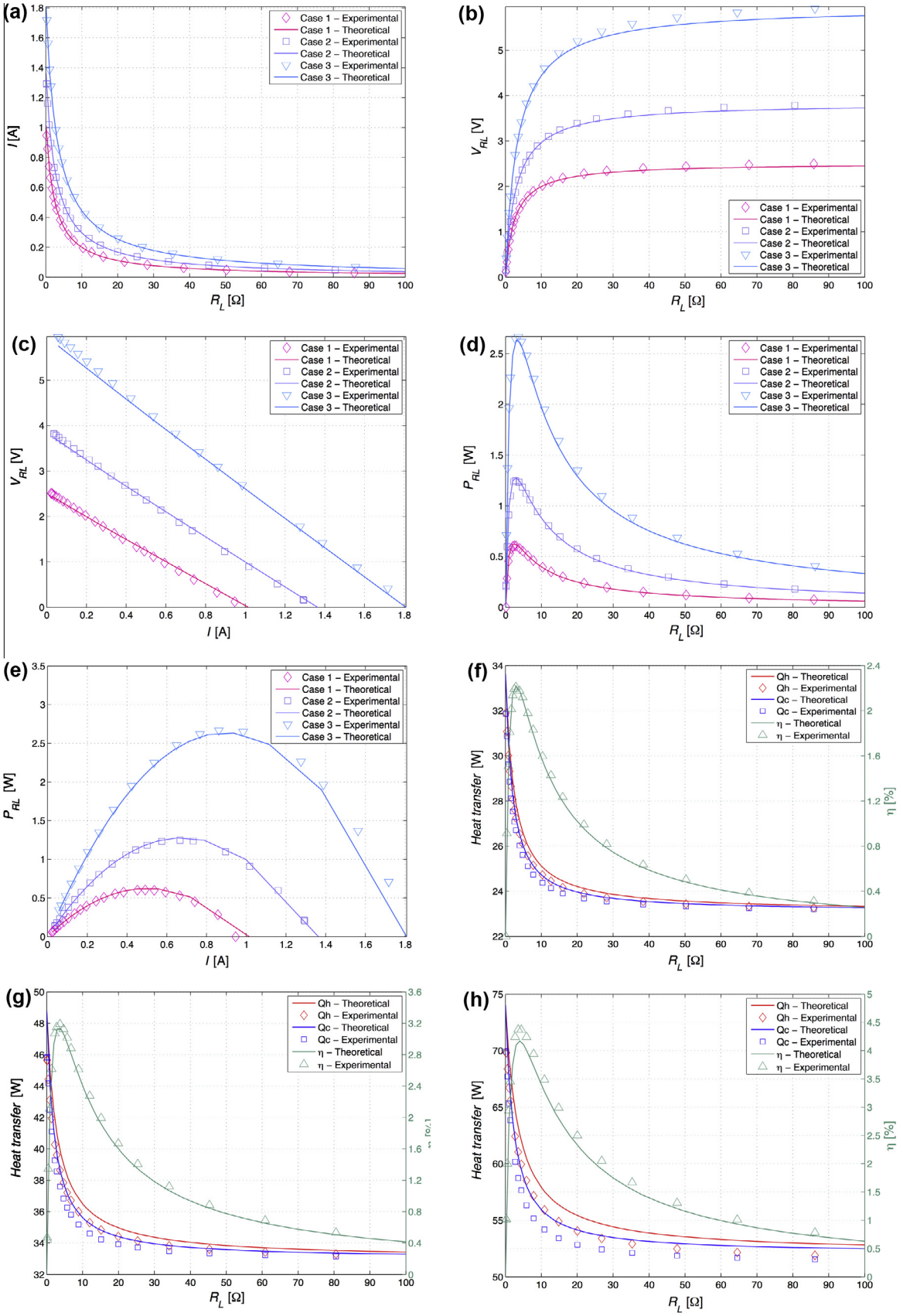

Fig. 6. Correlation of experimental and simulated behaviours of the TEG system under different load resistances. (a) Load current. (b) Closed-circuit voltage. (c) Closed-circuit voltage versus load current. (d) Electric output power. (e) Electric power generated versus load current. (f)–(h) Hot and cold side heat fluxes and system efficiency.

steady state is achieved. It demonstrates that when load resistance R_L increase, the load current I falls to minimum, which reduces the Joule and Peltier effect of the Eqs. (25) and (26). Consequently, when load current is very low, those effects are despicable and it is only the Fourier's law that governs the heat transfer equation.

4.4. Model uncertainty

The TEG model developed in this work is validated by comparing the experimental data with the numerical data predicted by our model at the same conditions. The calculus of the error is performed by the comparison of the temperature difference and the electrical output power of each point predicted by the model with the same point measured experimentally. The value of RMSE is 4.85 °C and 0.0648 W for temperature difference and electrical output power, respectively. The model presents a normalized root mean square error of 3.53% and 2.33% for temperature difference and electrical output power, respectively.

Although the model presented has slightly higher temperature difference RMSE and NRMSE than the model developed by Montecucco [15] (3.58 °C and 2.76%, respectively), the output power prediction is significantly better (0.2 W and 4.55%, respectively). It is important to note that the model accuracy is markedly affected by the thermoelectric parameters introduced into the simulation model. Consequently, the more exact the thermoelectric parameters are, the more precise the outputs will be.

5. Conclusions

Although thermoelectric phenomena have been used for heating and cooling applications quite extensively, electricity generation has only seen very limited market in niche applications and it is only in recent years that interest has increased regarding new applications of energy generation through thermoelectric harvesting. The widespread use of TEGs depends on its optimization.

The TRNSYS component presented in this paper has been developed for this purpose and is described and validated using experimental data. The proposed component is able to cope with thermal and electrical dynamics. The comparison of results between theoretic analysis and experiment has approved the reasonability of the new component.

On the other hand, the TRNSYS simulation runs without interruptions or delays, therefore the numerical model, and consequently the new component, can be considered well optimized. Therefore, this system model can be used in performance optimization and further application of thermoelectric generation.

Acknowledgments

This work has been partially funded by the Generalitat de Catalunya under Grant No. 2009.SGR-374 and the MICINN-FEDER under Grants Nos. FIS-2009-13050 and FIS-2012-31307. Authors would also like to thank Association of Industrial Engineers of Catalonia (AEIC) for they partial financial support.

References

[1] Riffat SB, Ma X. Thermoelectrics: a review of present and potential applications. Appl Therm Eng 2003;23:913–35.
[2] Omer SA, Infield DG. Design and thermal analysis of two stage solar concentrator for combined heat and thermoelectric power generation. Energy Convers Manage 2000;41:737–56.
[3] Risse S, Zellbeck H. Close-coupled exhaust gas energy recovery in a gasoline engine. Res Therm Manage 2013;74:54–61.
[4] Wang Y, Dai C, Wang S. Theoretical analysis of a thermoelectric generator using exhaust gas of vehicles as heat source. Appl Energy 2013;112:1171–80.
[5] Weng Chien-Chou, Huang Mei-Jiau. A simulation study of automotive waste heat recovery using a thermoelectric power generator. Int J Therm Sci 2013;71:302–9.
[6] Champier D, Bédécarrats J, Kousksou T, Rivaletto M, Strub F, Pignolet P. Study of a TE (thermoelectric) generator incorporated in a multifunction wood stove. Energy 2011;36:1518–26.
[7] Venkatasubramanian R, Siivola E, Colpitts T, O'Quinn B. Thin-film thermoelectric devices with high room-temperature figures of merit. Nature 2001;413:597–602.
[8] Boukai AI, Bunimovich Y, Tahir-Kheli J, et al. Silicon nanowires as efficient thermoelectric materials. Nature 2008;451:168–71.
[9] Hsiao YY, Chang WC, Chen SL. A mathematic model of thermoelectric module with applications on waste heat recovery from automobile engine. Energy 2010;35:1447–54.
[10] Chen L et al. Effect of heat transfer on the performance of thermoelectric generators. Int J Therm Sci 2002;41:95–9.
[11] Ebling D et al. Multiphysics simulation of thermoelectric systems for comparison with experimental device performance. J Electron Mater 2009;38(7):1456–61.
[12] Gou X, Yang S, Xiao H, Ou Q. A dynamic model for thermoelectric generator applied in waste heat recovery. Energy 2013;52:201–9.
[13] Montecucco A, Buckle JR, Knox AR. Solution to the 1-D unsteady heat conduction equation with internal Joule heat generation for thermoelectric devices. Appl Therm Eng 2012;35:177–84.
[14] Nguyen NQ, Pochiraju KV. Behaviour of thermoelectric generators exposed to transient heat sources. Appl Therm Eng 2013;51:1–9.
[15] Montecucco A, Knox AR. Accurate simulation of thermoelectric power generating systems. Appl Energy 2014;118:166–72.
[16] Meng FK, Chen LG, Sun FR. A numerical model and comparative investigation of a thermoelectric generator with multi-irreversibilities. Energy 2011;36:3513–22.
[17] Klein SA et al. TRNSYS 16: A Transient System Simulation Program. USA: University of Wisconsin; 2006.
[18] Cheng CH, Huang SY, Cheng TC. A three-dimensional theoretical model for predicting transient thermal behavior of thermoelectric coolers. Int J Heat Mass Transf 2010;53:2001–11.
[19] Rodríguez A, Vián JG, Astrain D, Martínez A. Study of thermoelectric systems applied to electric power generation. Energy Convers Manage 2009;50:1236–43.
[20] Kim S. Analysis and modeling of effective temperature differences and electrical parameters of thermoelectric generators. Appl Energy 2013;102:1458–63.
[21] Gou X, Xiao H, Yang S. Modeling, experimental study and optimization on low-temperature waste heat thermoelectric generator system. Appl Energy 2010;87:3131–6.